NUMERICAL INVESTIGATION OF FORCED IGNITION IN LAMINAR COUNTERFLOW NON-PREMIXED METHANE-AIR FLAMES

E. RICHARDSON

E. MASTORAKOS

Hopkinson Laboratory, Department of Engineering, University of Cambridge, Trumpington Street, Cambridge, CB2 1PZ, U.K.

Corresponding author E. Mastorakos
Hopkinson Laboratory, Department of Engineering,
University of Cambridge, Trumpington Street,
Cambridge, CB2 1PZ, U.K.
Tel.: +44 (0)1223 332690, Fax: +44 (0)1223 332662
E-mail: em257@eng.cam.ac.uk

Running Title

Forced ignition of laminar non-premixed flames

ABSTRACT

Simulations of forced ignition of non-premixed laminar counterflow flames are used to study the effect of strain rate on ignition success. A one dimensional calculation is performed, using detailed methane chemical kinetics and treating the spark as an instantaneous heat release in an inert mixing layer. Ignition success depends on the mixture composition at the spark location, resulting in lean and rich ignitability limits for a given spark that can be different from the fuel's static flammability limits. The difference is attributed to the finite spark width and the diffusion of heat from the spark to the flammable mixture. Ignition is prohibited by excessive strain rates, in some cases at levels well below the extinction value. The structure of the evolving flame is examined in terms of temperature, heat release rate and species mass fraction distributions. In the case of successful ignition, the high temperature reached due to the spark energy deposition causes local auto-ignition and subsequently, intense burning rapidly consumes the premixed reactants in the mixing layer and a non-premixed flame survives. In the case of unsuccessful ignition, despite the auto-ignition achieved in the sparked region, the strain rate is sufficiently high or the composition is sufficiently far away from the nominally flammable mixture for the heat and radicals to diffuse without resulting in a flame at long times from the spark event.

Keywords: Forced ignition, laminar flames, simulations.

INTRODUCTION

An improved understanding of mixture ignitability is needed for the satisfactory treatment of forced ignition in flows with wide variations in fuel concentration. Gas turbine combustors and atmospheric releases of flammable material provide important examples of such flows. In laminar flows, the ignition success may have a probabilistic nature attributable to the randomness in the ignition system (Kono et al., 1984). In turbulent non-premixed flows, the mixture fraction fluctuations introduce the main stochasticity in ignitability (Birch and Lefebvre, 1979 and Alvani and Fairweather, 2002), and the ignition probability in turbulent non-premixed jets has been successfully correlated with the probability of finding flammable mixture at the spark location. However, measurements of spark ignition in a turbulent flow show a number of fluid dynamic influences in addition to the compositional effects. These include dependence on turbulence levels and on flow speed (Ballal and Lefebvre, 1977 and Ahmed and Mastorakos, 2005). Hence, a greater clarification of the effect of the flow on ignition of non-premixed flames is needed.

Rashkovsky (1999) analyzed numerically and with simple chemistry spark ignition of laminar non-premixed counterflow flames. He demonstrated that ignition, initiated by a hot gas kernel placed somewhere in the mixture, fails below a critical value of the Damköhler number. Direct Numerical Simulations of ignition in a turbulent fuel-air mixing layer (Chakraborty and Mastorakos, 2005), also with one-step chemistry, showed the development of a tribrachial structure, consistent with Ray et al. (2001), and demonstrated that intense turbulence may not allow the spark to develop into a flame. Detailed chemistry simulations have not been performed yet for laminar non-premixed flame ignition and it is not fully clear what is the maximum strain rate for successful ignition.

The laminar counterflow configuration provides a well-defined flow field in which to examine the effect of strain on flame structure and it is used here for studying forced ignition processes. Forced ignition is instigated by a heat source (igniter), which can take a variety of forms, including heated surfaces, electrical sparks and laser pulses. Even igniters of the same type can have very different characteristics in terms of the spatial and temporal evolution of the energy input. An idealised thermal analysis of spark ignition (Zeldovich, 1941 and Blanc et al., 1949) leads to the concept of a minimum ignition energy and to a minimum spark radius for ignition of the order of the premixed flame thickness (Glassman, 1987). Measurements of minimum ignition energy, around 0.30 mJ for stoichiometric methane-air mixtures (Kutcha), usually refer to the electrical energy provided to the spark electrodes. The energy retained by the flame kernel after conductive, acoustic and radiative losses is typically 2-16 % (Zeldovich, 1941) of this electrical energy. Alternative sparks include Laser Induced Spark Ignition that delivers a measurable quantity of energy to the fluid at the focus of the laser beam over a relatively short period of time, 5-500 ns (Phuoc, 2002). However, all types of sparks include complicated flow patterns, ionization, and shock waves (Kono et al., 1984 and Bradley et al., 2004) and are hence not easy to represent numerically, although the discharge phase following breakdown has been successfully modeled (Thiele et al., 2002).

In this paper, simulations of ignition in a laminar methane-air counterflow mixing layer have been performed in order to display the variety of ignition behaviour possible for a range of strain rates. The spark is modelled as a region of hot inert gas with a finite thickness. Details of the flow and ignition formulation are given in the following section. The resulting ignitability limits are then discussed, and the transient flame structures are examined. Where topogical effects such as flame curvature may be neglected, similar flame structures can be expected during the ignition of non-premixed turbulent flows.

FORMULATION

Configuration and computational code

The computational configuration is a non-premixed counterflow arrangement with planar geometry. RUN1DL is used to solve a low Mach number formulation of the flame equations in terms of a distance variable (ROTEXO, 2005), including detailed molecular transport. Variable molecular properties and the GRI-Mech 3.0 detailed chemical scheme are employed for reactions between methane and air (Gardiner et al.). The 53 species GRI-Mech 3.0 has been optimised for combustion of natural gas using data in the range 1000-2500 K, and shows realistic extinction behaviour.

The system of equations is integrated on an adaptive grid with a modified Newton method (ROTEXO, 2005), while ensuring grid independence of the solution. The fuel and air inlets are at y=-6 mm and y=6 mm respectively, and the boundary temperature and pressures are 293 K and 100 kPa. In the partially premixed flames examined, the air volume fraction in the fuel stream, X, was 0.8, while the non-premixed case uses streams of pure methane (i.e. X=0) and pure air. For X=0, the stoichiometric mixture fraction is $Z_{st}=0.055$, while for X=0.8, $Z_{st}=0.452$. The stagnation point is fixed at y=0 mm and the inlet velocities are determined according to a specified strain rate S. The values of mixture fraction used to report data from the counterflow calculations are calculated using nitrogen atom conservation. The static lean and rich flammability limits of ignition of homogeneous methane-air mixtures are, respectively, fuel volume fractions of 5% and 15% (Mallickrodt Baker, 2004), which translate to $Z_{lean}=0.0284$ and $Z_{rich}=0.089$ for X=0 and $Z_{lean}=0.233$ and $Z_{rich}=0.732$ for X=0.8. The strain rate at which the flame extinguishes is found to be $S_{ext}=475\ s^{-1}$ for the non-premixed case (X=0) and $S_{ext}=756\ s^{-1}$ for X=0.8, to within $1\ s^{-1}$.

Spark representation

The spark is assumed to cause instantaneous heating of a slab with thickness $\Delta\ y_{sp}$=0.25 mm centred at y_{sp}. The peak temperatures T_{sp} used were 3000 K and 4000 K and a smooth but very thin interface between the spark and the surrounding inert fluid is used to avoid numerical problems initially. The spark temperatures used correspond to a constant pressure heat addition of 429 kJ m^{-3} and 558 kJ m^{-3} (Vargaftik, 1975) based on the spark volume, hence the 4000 K spark contains about 30 % more energy than the 3000 K spark. Repeating Glassman's (1987) idealized spark analysis for this one dimensional problem, one obtains that the critical spark half-width for successful ignition $r_f \geq \sqrt{\pi}\ \delta \approx 1.8\delta$, where $\delta = \alpha/S_L$. This contrasts with $r_f \geq 3.7\delta$ for the radius of a spherical spark (Glassman, 1987). Using the thermal diffusivity for air $\alpha = 2.15 \cdot 10^{-5}\ m^2 s^{-1}$ (Vargaftik, 1975), and calculating methane's stoichiometric laminar flame speed as $S_L = 0.37\ m\ s^{-1}$ from the code (ROTEXO, 2005) with the same chemistry at 293 K and 1 bar, the critical heat input width for the one-dimensional problem may be estimated as 0.2 mm. Therefore the spark width considered in this work is slightly larger than the critical spark width for successful premixed ignition. In addition, considering the fact that our spark temperature is higher than the adiabatic flame temperature of stoichiometric methane-air flames, we conclude that our spark representation ignites safely a homogeneous stagnant stoichiometric mixture. This has also been demonstrated by separate runs of RUN1DL.

The initial condition used is a converged inert flow with the spark's temperature profile subsequently imposed. The low Mach number formulation in RUN1DL does not capture pressure waves that may result from sudden temperature changes, nor is the chemical mechanism reliable at the high initial temperatures. Therefore the early evolution of the chemical composition and of the velocity field should not be given undue credence, however the total spark energy is still conserved. The temperature falls rapidly and subsequent predictions are more credible.

RESULTS AND DISCUSION

Ignition limits

Figure 1 shows the evolution of the temperature profile during successful ignition of a non-premixed flame. The mixture at the centre of the spark is lean. The peak temperature has decreased from 4000 K to 3848 K within $2.0{\cdot}10^{-7}$ s due to diffusion of the spark and an initial predominance of endothermic reactions. As the heat release increases, the peak temperature rises to 3868 K at $1.0{\cdot}10^{-6}$ s. Heat from the flame diffuses through the mixing layer, while the spark energy is dissipated, and a steady diffusion flame has been established by $1.0{\cdot}10^{-2}$ s. In the following, successful ignitions are deemed only the simulations that result in similar non-premixed flames after steady-state has been achieved.

A large number of ignition simulations were performed across a range of strain rates and spark positions. The resulting loci of mixing layer ignitability limits are shown in Fig. 2 for the non-premixed case with 3000 K and 4000 K sparks. Figure 3 shows the ignitable region for T_{sp}=3000 K sparks in the partially premixed case. In both figures, the position coordinate has been transformed using the factor $(S/S_{ext})^{1/2}$, which is proportional to the physical width of the inert mixing layer (Pitsch and Peters, 1998). Through this transformation, contours of mixture fraction become vertical lines. The loci of stoichiometry and of the premixed static flammability limits \cite{limits} are shown for comparison. Figure 2 also shows the locations of three 4000 K sparks labeled as A-C (Table 1), examined in greater detail later. Sparks A and C are outside the ignitable region, while B results in the steady diffusion flame seen in Fig. 1.

Sparks centred within the closed region in Figs. 2 and 3 result in successful ignition, while sparks outside this region do not lead to ignition. Ignition only occurs for sparks falling within a range of mixture fraction and below a certain strain rate. It can be possible to ignite the flow despite sparking at a non-flammable mixture fraction because sufficient heat and reactive species may still diffuse into the flammable region to lead to a sustainable flame. As the strain rate increases the mixing layer becomes narrower. At the extinction value of S=756 s^{-1} (for the X=0.8 flame), the width of the fluid slab between the static flammability limits is

0.225 mm, which is just less than the width of the spark. Thus, when the spark's centre lies outside the nominally flammable region there can still be a degree of overlap between the spark and the flammable region. Therefore, because in reality sparks have finite size, the presence of nominally flammable mixture at the spark centre is not necessarily a requirement for ignition. The fact that the ignitability limit is wider than the region bounded by the static flammability limits in Fig. 2 is consistent with the observed increased probability of igniting a non-premixed turbulent jet flame by increasing the spark size (Ahmed and Mastorakos, 2005).

It is not possible to ignite a stable flame when the global strain rate is above the extinction strain rate S_{ext}. However, in the flame with X = 0, ignition did not occur above 45 % of the extinction strain rate with the 3000 K spark and not above 50 % of S_{ext} for T_{sp} = 4000 K. It may be expected that further increases in the spark energy will increase the maximum ignitable strain rate until it coincides with the extinction strain rate. The ignitable region for T_{sp} = 3000 K is completely within the ignitable area for T_{sp} = 4000 K. Not only does increasing the spark energy make it possible to ignite at higher strain rates, it also increases the range of mixture fractions (e.g. the loci in Fig. 2 become wider with T_{sp}).

In the laminar counterflow configuration, both extinction and the quenching of an otherwise viable ignition kernel are largely controlled by the strain rate S. As a consequence, the critical strain rate of extinction and the critical strain rate of forced ignition could be expected to follow similar trends as the boundary conditions are changed, for example by increased premixing or inlet temperatures. In agreement with previous findings (e.g. Pitsch and Peters, 1998), the partially premixed flow has a higher extinction strain rate than the non-premixed flow (calculated as 756 s^{-1} compared to 475 s^{-1}). Indeed, for the 3000 K spark, a comparison between Fig. 2 and 3 shows that this spark is sufficient to ignite a partially-premixed flame up to the extinction strain rate, but it is sufficient to ignite the pure diffusion flame only for S up to 45 % of S_{ext}.

In Figs. 2 and 3, the ignitability limits are not symmetrical about stoichiometry. In the non-premixed case, ignitability is favoured at lean mixture fractions as the strain rate is increased, while rich mixtures show greater ignitability in the partially premixed case. This is best understood through a consideration of the scalar dissipation profile in a counterflow. The scalar dissipation peaks close to the stagnation point (at $y = 0$ and a mixture fraction of $Z = 0.5$) and so, for the $X = 0$ case, a spark in a lean region ($Z < Z_{lean}$) experiences a smaller scalar dissipation than a spark in the rich region ($Z > Z_{rich}$). This implies a greater resilience of the lean spark for the same strain rate. For the partially premixed flame, $Z_{st} = 0.452$ and there is little difference in the scalar dissipation rate experienced by a lean and a rich spark. Hence the difference between the distances separating the ignitability limits from their respective flammability limits is less. However, Fig. 3 indicates that ignition of rich mixtures is more resilient to the effects of strain rate than ignition of lean mixtures for $X=0.8$. The fact that the rich ignitability contour is sloping to the left may be attributed to the increasing overlap between the spark and the flammable region as the mixing layer gets thinner, off-setting the adverse effects of increased strain. The fact that the lean ignitability limit also slopes to the left implies an additional chemical effect making the richer sparks more resilient to the dissipative effects of strain.

Ignition Evolution

It has been seen that both strain and composition influence the survival of an ignition kernel. This section examines the detailed evolution of the kernel following the spark in the non-premixed flame. Figure 4 shows transient temperature profiles for sparks A, B and C in mixture fraction space. Spark A is located at a sufficiently lean mixture fraction that by the time appreciable spark energy arrives in the flammable region, the temperature has decreased too much for successful ignition. Spark B is successful. Spark C fails to ignite despite sparking the entire flammable region. While spark C seems more promising than the leaner spark B, it should be noted that the scalar dissipation rate gets higher closer to the stagnation point where $Z = 0.5$ and this apparently leads to the quenching of spark C.

In case A, the consumption of oxygen and methane is very limited (Fig. 5). In case B, the reactants are initially consumed in the region of the spark and subsequently the premixed reactants from outside the spark region are consumed until a diffusion flame is achieved. The flame structure during this premixed phase is not clear from Fig. 5, however it involves flame fronts propagating across the mixing layer away from the spark. The flame front fades as it reaches very rich or very lean mixtures, but these transient reaction zones are evident in mixtures quite far from the static flammability limits. In case C, a large proportion of the reactants is consumed within the spark region, however there is greater fuel leakage than in case B. Consumption of the surrounding cold premixed reactants proceeds, but the flame is quenched before the stable diffusion flame condition is achieved.

The initial, strongly endothermic heat release seen in Fig. 6 is very short lived ($t < 10^{-6}$ s) and is replaced by an exothermic heat release profile with two peaks close to the rich and lean edges of the spark. While the small physical size of the inflamed region may make it inappropriate to discuss individual flame fronts, the large heat release rates at the edges of the burning regions, rather than close to stoichiometry early on, indicate that premixed type reaction zones dominate for around $2.0 \cdot 10^{-4}$ s. For successful ignition it is then necessary to stabilise a diffusion flame, as is seen in the case of spark B. The flame structure involving rich and lean fronts and an inner diffusion flame may be described as tribrachial (Buckmaster, 2002). The evolution of the OH concentration is reported in Fig. 7. In agreement with experimental observations (Thiele et al., 2002), the predicted transient OH concentration peaks at around an order of magnitude higher than in the steady diffusion flame and then it decays while the temperature falls. The shape of the OH profile reflects that of the temperature, rather than the heat release.

The same qualitative behaviour can be observed for the differences between a successful and an unsuccessful spark for the partially-premixed case. Figure 8 shows that the initial heat from the spark diffuses into the unburnt mixture and eventually a flame is established for Spark E, whilst the spark is quenched in the other two cases. Distinct premixed flame fronts are not as visible here as for $X = 0$ due to the large width of the diffusion-flame reaction zone in Z-space for large air premixedness. However, the heat release profiles (Fig. 9) at early times show evidence of two peaks corresponding to the edges of spark. The heat release reaches high levels during the auto-ignition phase of the sparked region, but these quickly decay to zero in the case of failed sparks and to the much lower values (hardly visible with the scale of Fig. 9) associated with a non-premixed flame at Z_{st} in the case of successful sparks.

The OH mass fraction profile in the flame with X = 0.8 (Fig. 10) shows that the OH has very small concentrations at $t = 2.0 \cdot 10^{-7}$ s, but it then increases rapidly for all sparks and auto-ignition has occurred by $t = 2.0 \cdot 10^{-6}$ s (see also the switch between negative to positive heat release in Fig. 9}). The OH then decays to virtually zero by $t=2.0 \times 10^{-4}$ s for the failed sparks, with a flame stabilized by $t=2.0 \times 10^{-3}$ s for the successful spark E. Again, super-equilibrium OH is observed initially due to the auto-ignition of the sparked mixture.

CONCLUSIONS

Calculations of non-premixed and partially premixed laminar counterflow flames with detailed chemistry have been performed with a simulated spark to understand the factors affecting ignition success in non-premixed combustion. The results showed that there is a critical strain rate, which depends on the igniter, above which forced ignition is impossible for all spark positions. This critical value can be less than the extinction strain rate at which a steady flame becomes impossible, even for a spark thickness and energy that would ignite a stoichiometric homogeneous mixture. For a particular spark position relative to the stoichiometric mixture, failure to ignite is due to a combination of excessive dissipation and the local mixture flammability. Regions of very low scalar dissipation rate can have insufficient fuel to ignite, while otherwise flammable regions can fail to ignite due to the local dissipation rate being too high.

The transient flame structure was analyzed during successful and unsuccessful ignition. Once reactants have been consumed in the ignition region, premixed flame fronts develop to consume the partially-premixed fluid. As the spark heat is diffused, the premixed fronts become less distinct and finally a non-premixed flame is stabilized.

Acknowledgments

This work has been funded by the Engineering and Physical Sciences Research Council and Rolls-Royce (UK).

REFERENCES

Ahmed, S.F., and Mastorakos, E. (2005) Measurements of the probability of ignition and subsequent flame propagation speed in turbulent non-premixed jets, In *Proc. 20th ICDERS*, Montreal.

Alvani, R.E., Fairweather, M., (2002) Ignition Characteristics of Turbulent Jet Flows. *Trans. of I Chem E*, 80, 917-923.

Ballal, D.R., and Lefebvre, A.H. (1977) Ignition and flame quenching in flowing gaseous mixtures**.** *Proc. R. Soc. Lond. A.*, 357, 163-181.

Ballal, D.R., and Lefebvre, A.H. (1979) Ignition and flame quenching of flowing heterogeneous fuel-air mixtures. *Combust. Flame*, 35, 155-168.

Blanc, M.V., Guest, P.G., von Elbe, G., and Lewis, B. (1946) Ignition of Explosive Gas Mixtures by Electric Sparks. I. Minimum Ignition Energies and Quenching Distances of Mixtures of Methane, Oxygen, and Inert Gases. *Proc. Combust. Inst.*, 3.

Bradley, D., Sheppard, C.G.W., Suardjaja, I.M., and Wooley, R. (2004) Fundamentals of high-energy spark ignition with lasers. *Combust. Flame*, 138, 55-77

Buckmaster, J. (2002) Edge-Flames. *Prog. Energ. Combust. Sci.*, 28, 435-475.

Chakraborty, N., and Mastorakos, E. (2005) Effects of turbulence on spark ignition in inhomogeneous mixtures: A direct numerical simulation (DNS) study. In *The Fourth Mediterranean Combustion Symposium*, Lisbon.

Gardiner, B., Yang, H., Qin, Z., Smith, G., Crosley, D., Golden, M., Bowman, C.T., Hanson, R., Davidson, D., Frenlach, M., Moriarty, N., and Eiteener, B., `http://me.berkeley.edu/gri_mech`.

Glassman, I. (1987) *Combustion*. Academic Press Inc., Orlando, Florida, Second edition.

Kono, M., Hatori, K., and Iinuma K. (1984) *Proc. Combust. Instit.*, 20, 133-140.

Kutcha, J.M. US Dept of the Interior Bureau of Mines Bulletin 680.

Mallickrodt Baker Inc. (2004) Material safety data sheet. Technical Report M2015, US Environmental Health and Safety.

Mastorakos, E., Taylor, A.M.K.P., and Whitelaw, J.H. (1992), Extinction and temperature characteristics of turbulent counterflow diffusion flames with partial premixing. *Combust. Flame*, 91, 40-54

Phuoc, T.X., White, C.M., and McNeil, D.H. (2002) Laser spark ignition of a jet diffusion flame. *Optics and Lasers in Engineering*, 38, 217-232.

Pitsch, H., Peters, N., (1998) A consistent flamelet formulation for non-premixed combustion considering differential diffusion effects *Combust. Flame*, 114, 26-40.

Rashkovsky, S.A. (1999), Spark ignition of ill-mixed gases. In *The First Mediterranean Combustion Symposium*, Antalya, 1403-1411.

Ray, J., Najm, H.N., and McCoy, R.B. (2001) Ignition front structure in a methane-air jet. In *2nd Joint Meeting of the U.S. Sections of the Combustion Institute*, 150.

Rotexo GmbH Co.KG, Haan, Germany (2005). *The Combustion Simulation Laboratory*, Version 1.3, `www.SoftPredict.com`.

Thiele, M., Warnatz, J., Dreizler, A., Lindenmaier, S., Schiebl, R., Maas, U., Grant, A., and Ewart, P. (2002) Spark ignited hydrogen/air mixtures: two dimensional detailed modeling and laser based dagnostics.*Combust. Flame*, 128, 74-87.

Vargaftik, N.B. (1975) *Tables on the Thermophysical Properties of Liquids and Gases*. John Wiley and Sons, Inc., New York, Second edition.

Zeldovich, Ya.B. (1941) *Zh. Eksp. Teor. Fiz.*, 11. See Shchetinkov, Ye.S. (1969) “The Physics of the Combustion of Gases”, Chapter 5, Edited Translation FTD-HT-23-496-68, Translation Revision, Foreign Technology Division, Wright-Patterson AFB, Ohio.

Table 1. Details for sparks A-F

	S (s^{-1})	y_{sp}(mm)	X	T_{sp}(K)	Success/Failure
Spark A	190.0	0.555	0	4000	F
Spark B	190.0	0.689	0	4000	S
Spark C	190.0	0.823	0	4000	F
Spark D	378.0	-0.169	0.8	3000	F
Spark E	378.0	0.029	0.8	3000	S
Spark F	378.0	0.229	0.8	3000	F

List of Figures

TY1.eps

Figure 1. Transient temperature profiles in physical space during a successful ignition event. Spark B from Table 1 LIM5.eps

Figure 2. The loci of the ignitability limits for 3000 K sparks (crosses) and 4000 K sparks (circles) for the X=0 flame. The stoichiometric mixture fraction and the static rich and lean flammability limits are indicated.

LIMSAM2.eps

Figure 3. The locus of the ignitability limits for 3000 K sparks in a flame with X=0.8. The stoichiometric mixture fraction and the static rich and lean flammability limits are indicated.

TZ2.eps

Figure 4. Transient temperature profiles in mixture fraction space for sparks A, B and C.

R3.eps

Figure 5. Transient mass fraction profiles in mixture fraction space for methane and oxygen for sparks A, B and C.

Q3.eps

Figure 6. Transient heat release profiles in mixture fraction space for sparks A, B and C. The inset graph is an enlargement showing the stabilised heat release profile for case B.

OHZ1.eps

Figure 7. Transient OH mass fraction profiles in mixture fraction space for sparks A, B and C.

samTZ1.eps

Figure 8. Transient temperature profiles in mixture fraction space for Sparks D, E and F.

samQ1.eps

Figure 9. Transient heat release profiles in mixture fraction space for sparks D, E and F.

samOHZ1.eps

Figure 10. Transient OH mass fraction profiles in mixture fraction space for sparks D, E and F.

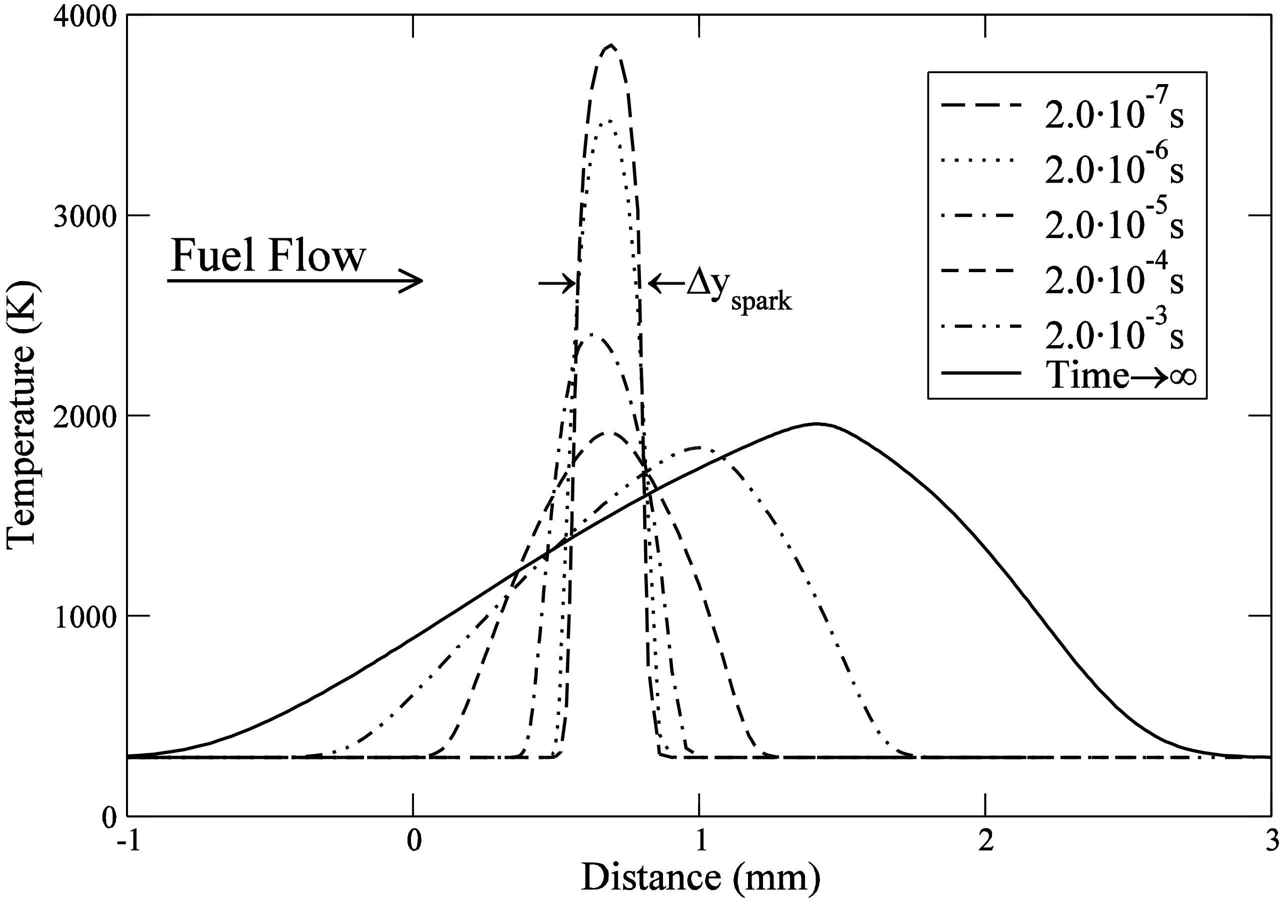
4000
3000
2000
1000
0
Temperature (K)
-1
0
1
2
3
Distance (mm)
Fuel Flow
Δy_{spark}
$2.0\cdot10^{-7}$s
$2.0\cdot10^{-6}$s
$2.0\cdot10^{-5}$s
$2.0\cdot10^{-4}$s
$2.0\cdot10^{-3}$s
Time→∞

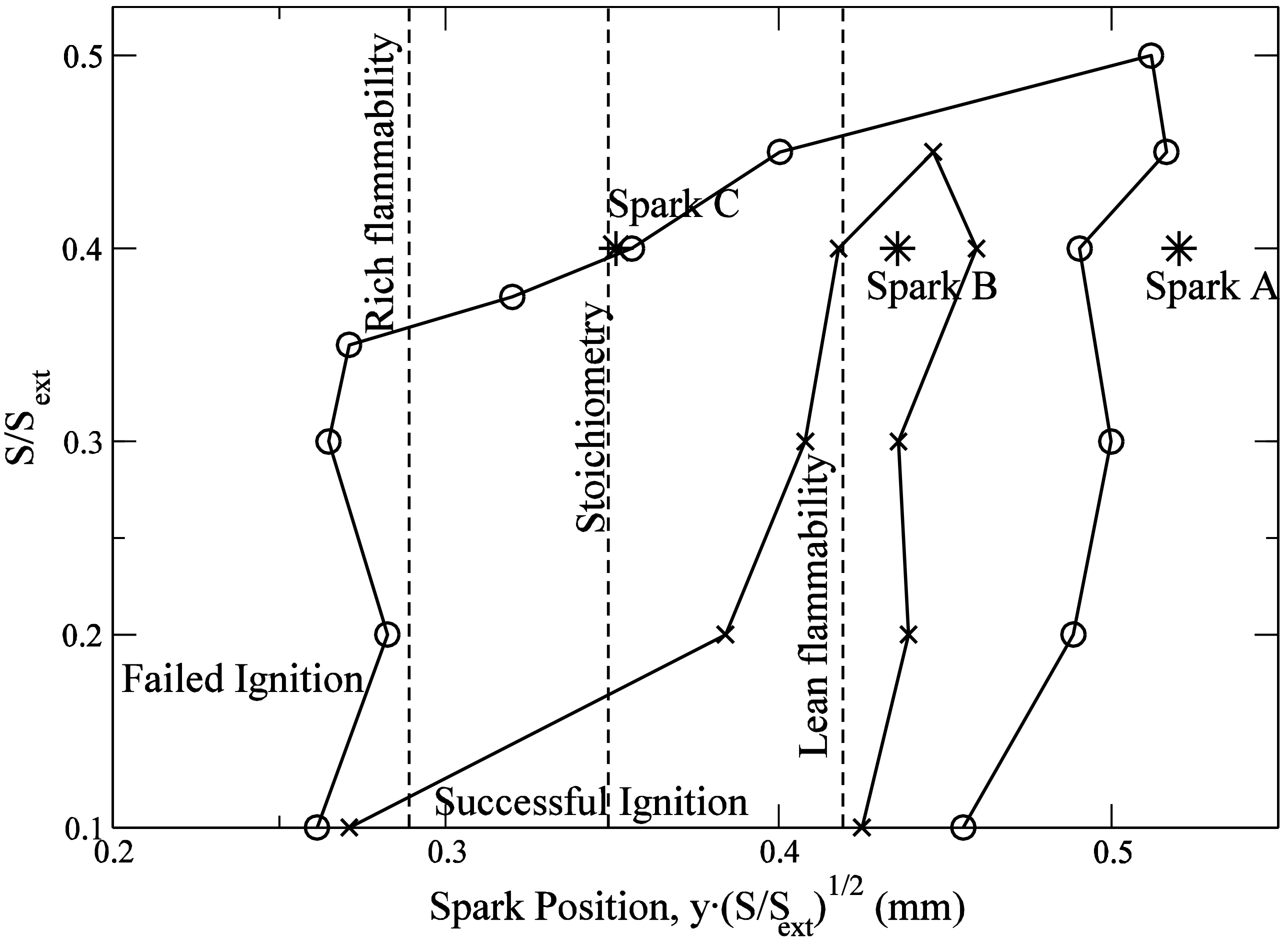

Rich flammability
Stoichiometry
Lean flammability
Spark C
Spark B
Spark A
Failed Ignition
Successful Ignition
S/S_{ext}
0.1
0.2
0.3
0.4
0.5
0.2
0.3
0.4
0.5
Spark Position, $y\cdot(S/S_{ext})^{1/2}$ (mm)

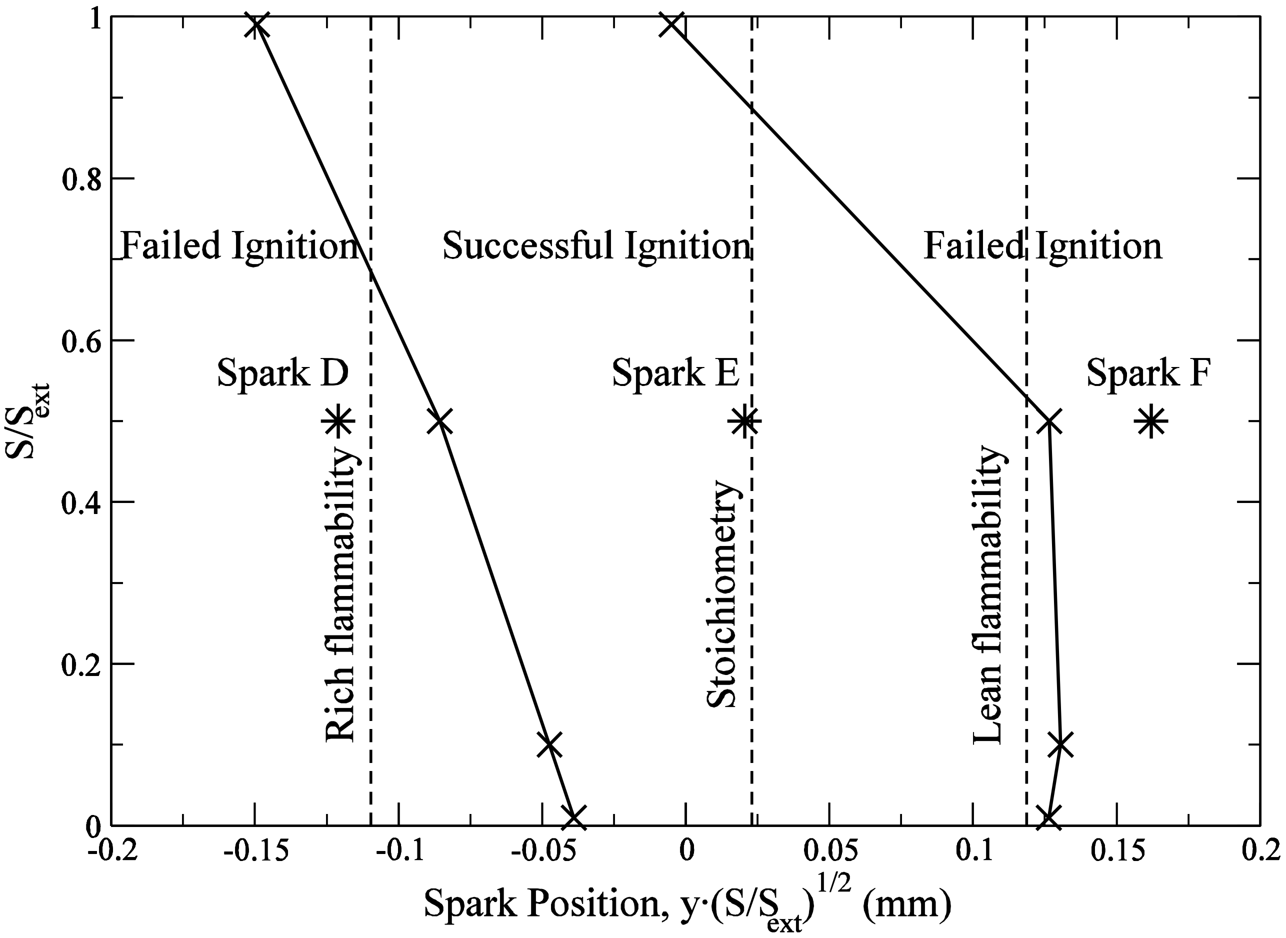

S/S$_{ext}$
Spark Position, y·(S/S$_{ext}$)$^{1/2}$ (mm)
Failed Ignition
Successful Ignition
Failed Ignition
Spark D
Spark E
Spark F
Rich flammability
Stoichiometry
Lean flammability
0
0.2
0.4
0.6
0.8
1
-0.2
-0.15
-0.1
-0.05
0
0.05
0.1
0.15
0.2

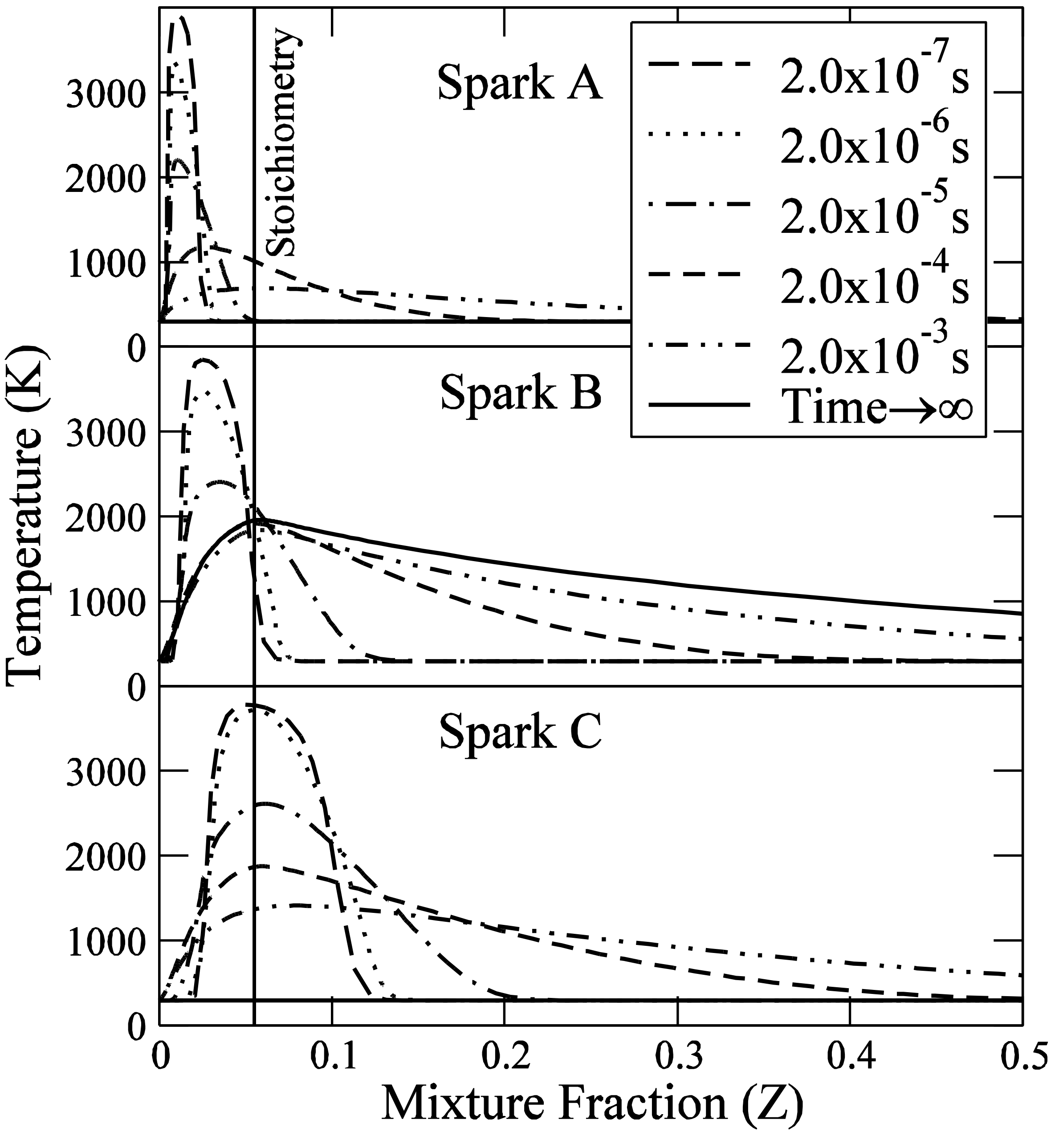
Spark A
Spark B
Spark C
Stoichiometry
2.0x10^{-7}s
2.0x10^{-6}s
2.0x10^{-5}s
2.0x10^{-4}s
2.0x10^{-3}s
Time→∞
Temperature (K)
0
1000
2000
3000
Mixture Fraction (Z)
0
0.1
0.2
0.3
0.4
0.5

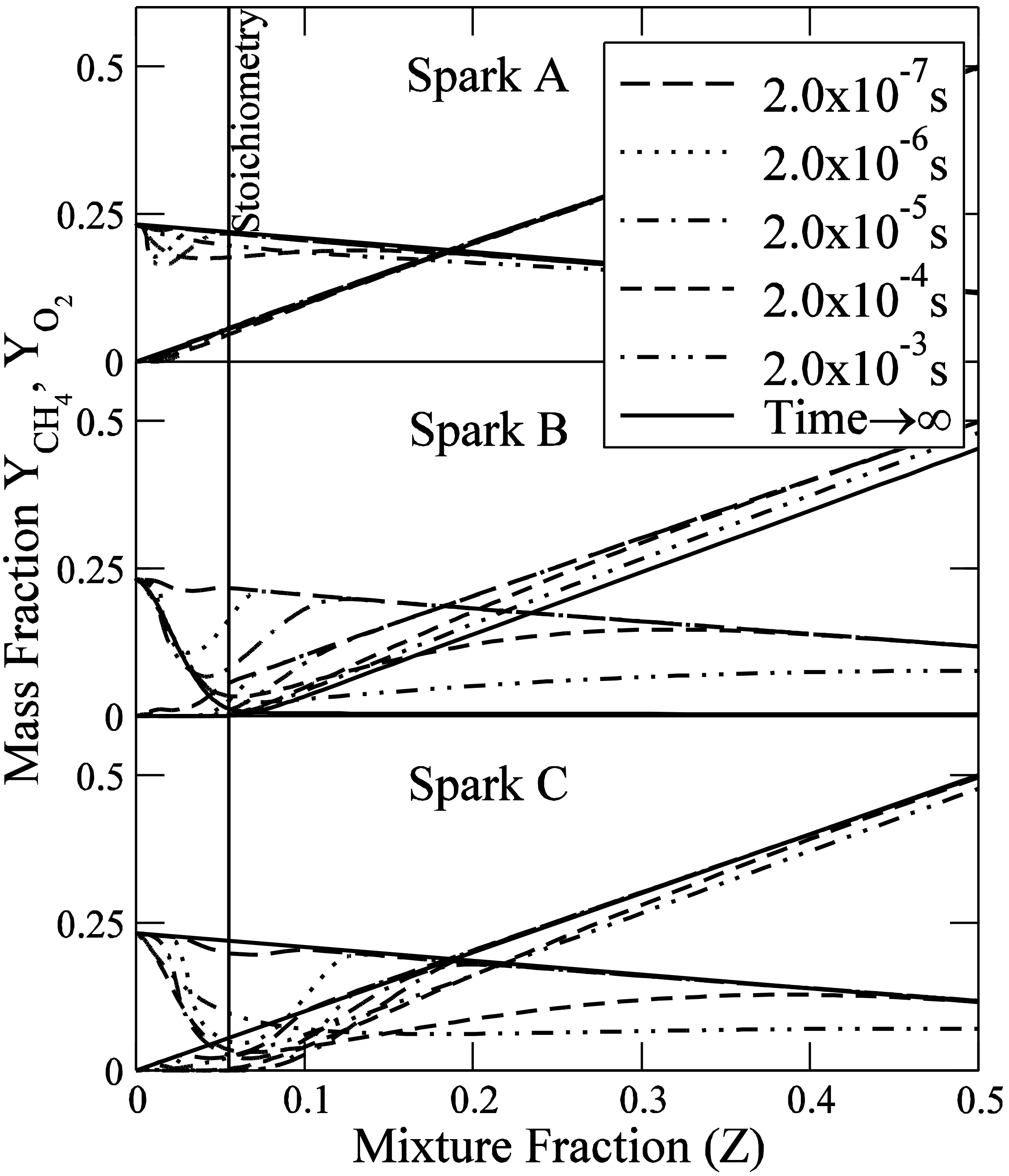
Spark A
Spark B
Spark C
Stoichiometry
2.0x10^-7 s
2.0x10^-6 s
2.0x10^-5 s
2.0x10^-4 s
2.0x10^-3 s
Time→∞
Mass Fraction Y_{CH_4}, Y_{O_2}
Mixture Fraction (Z)
0
0.25
0.5
0
0.1
0.2
0.3
0.4
0.5

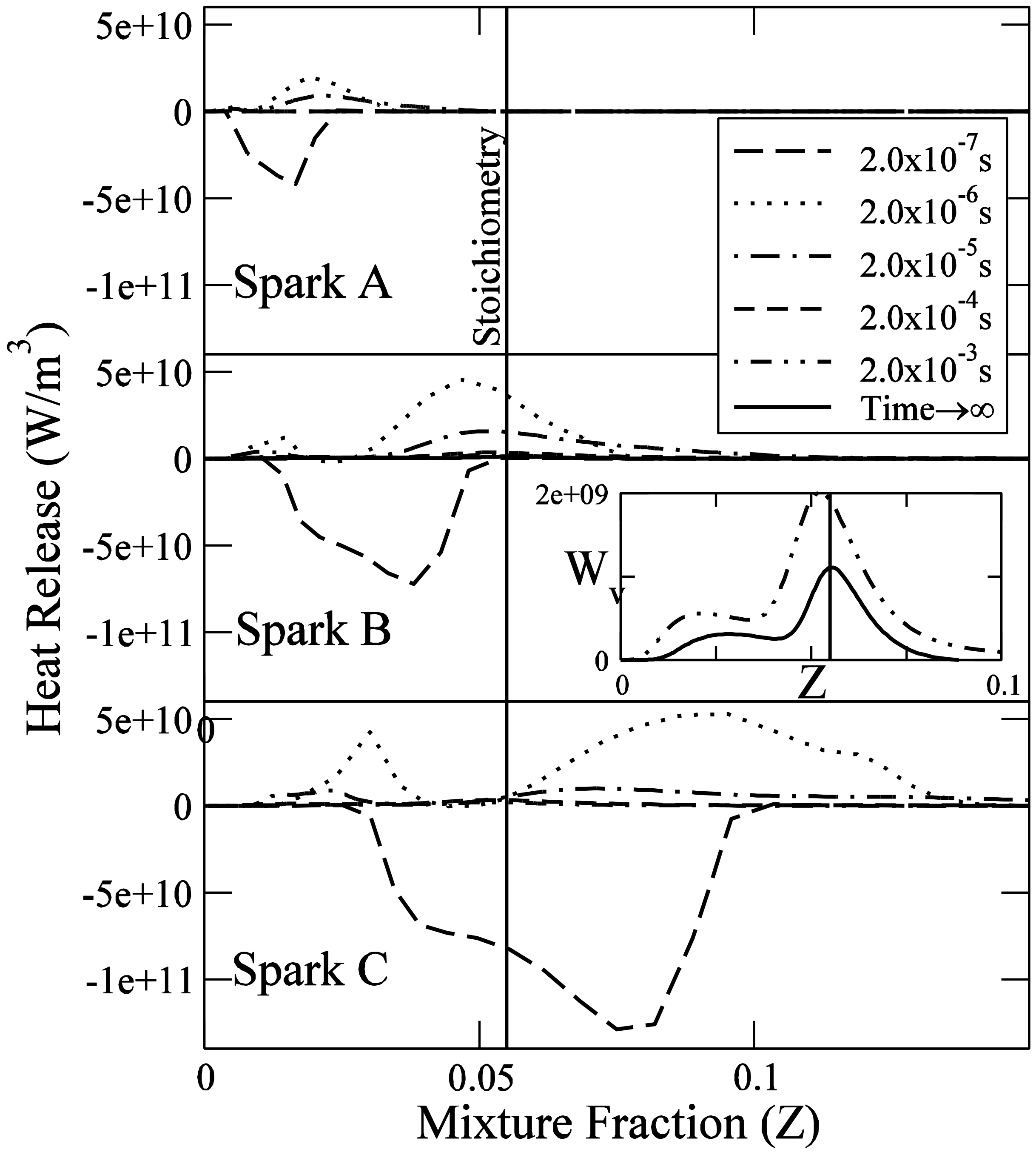

Heat Release (W/m^3)
5e+10
0
-5e+10
-1e+11
Spark A
Spark B
Spark C
Stoichiometry
2.0×10^{-7}s
2.0×10^{-6}s
2.0×10^{-5}s
2.0×10^{-4}s
2.0×10^{-3}s
Time→∞
2e+09
W_v
Z
0
0.1
0.05
Mixture Fraction (Z)

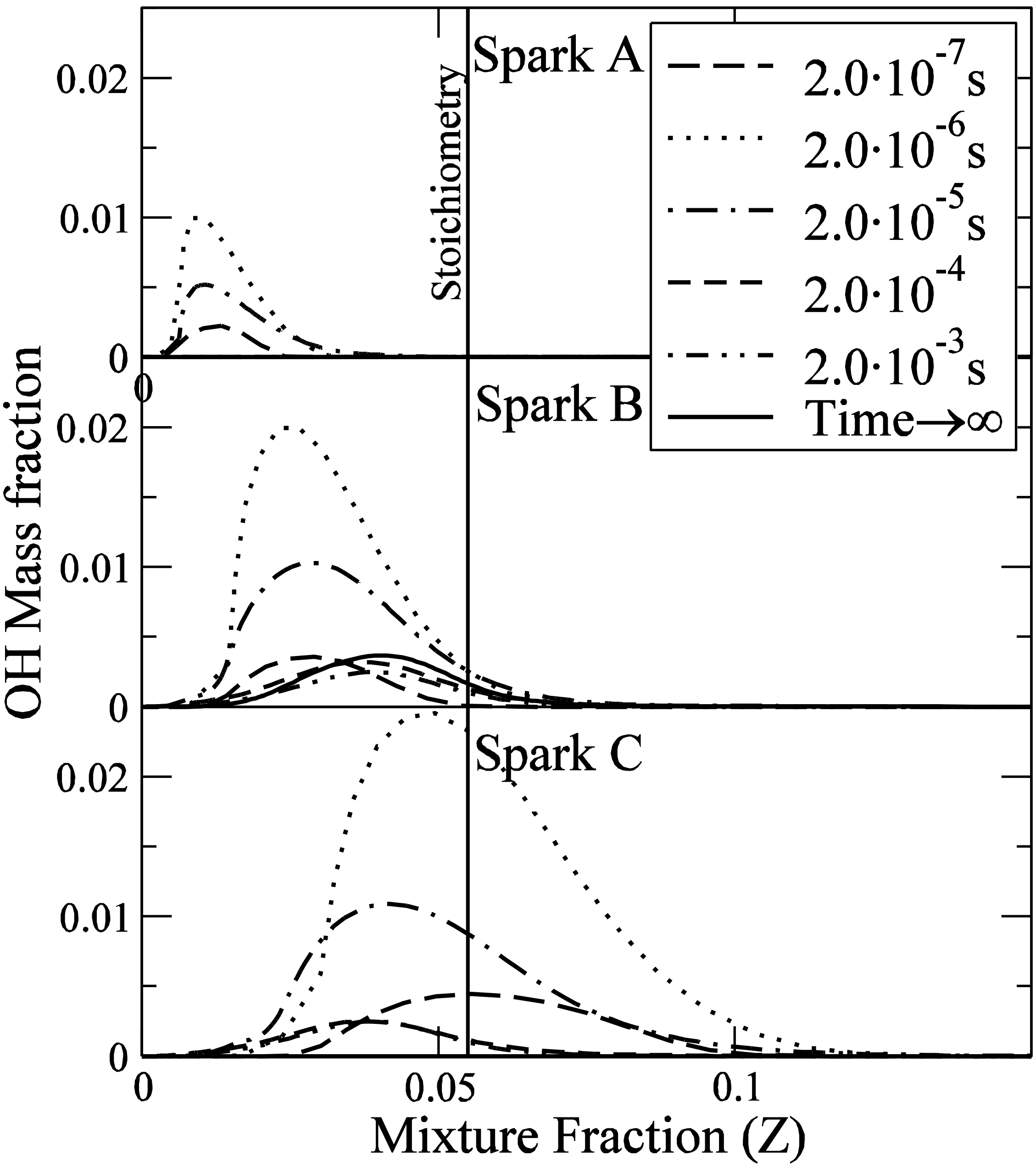

Spark A
Spark B
Spark C
Stoichiometry
$2.0\cdot10^{-7}$s
$2.0\cdot10^{-6}$s
$2.0\cdot10^{-5}$s
$2.0\cdot10^{-4}$
$2.0\cdot10^{-3}$s
Time→∞
OH Mass fraction
0.02
0.01
0
0
Mixture Fraction (Z)
0
0.05
0.1

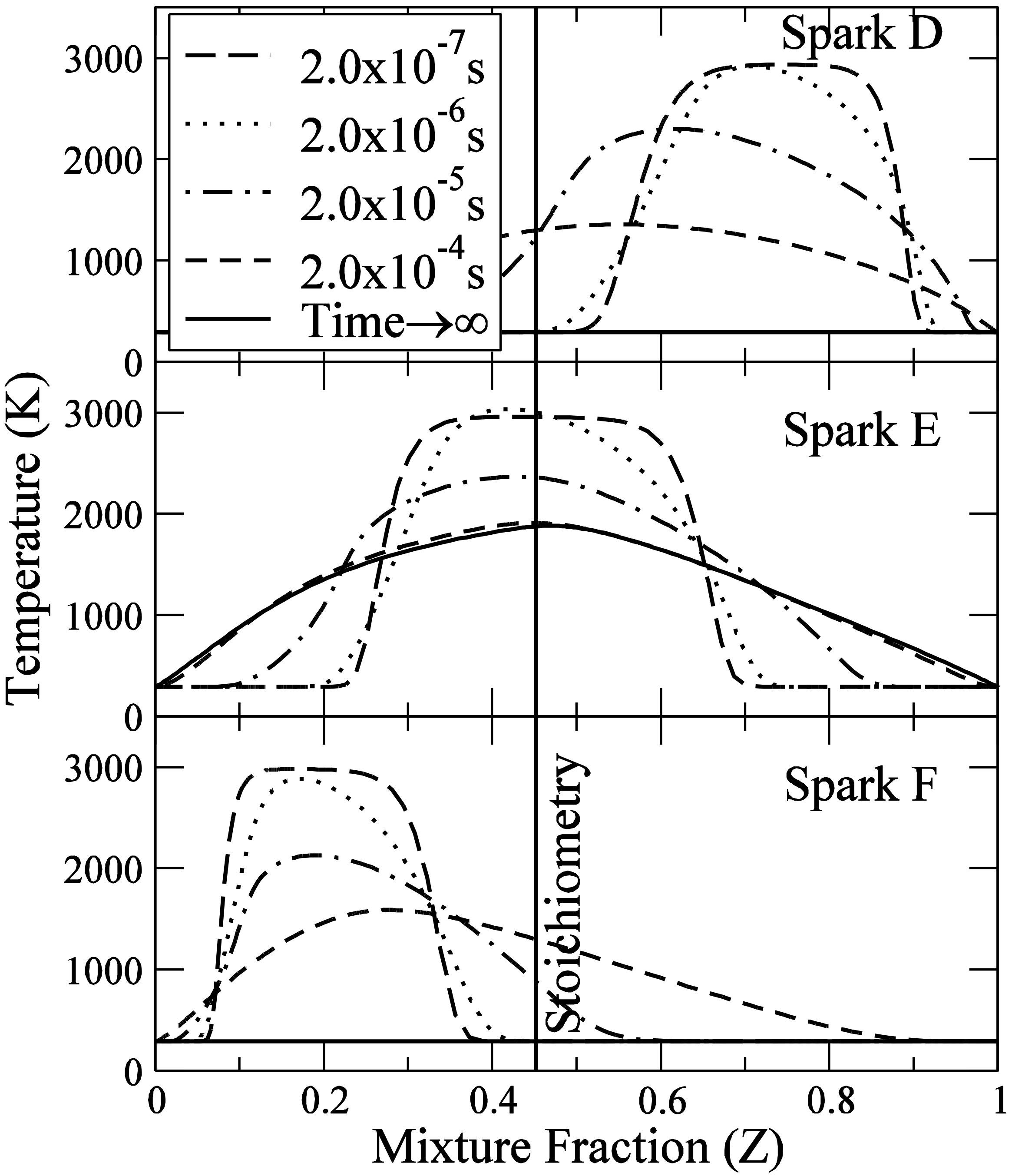

Spark D
Spark E
Spark F
2.0x10^{-7}s
2.0x10^{-6}s
2.0x10^{-5}s
2.0x10^{-4}s
Time→∞
Stoichiometry
Temperature (K)
0
1000
2000
3000
Mixture Fraction (Z)
0
0.2
0.4
0.6
0.8
1

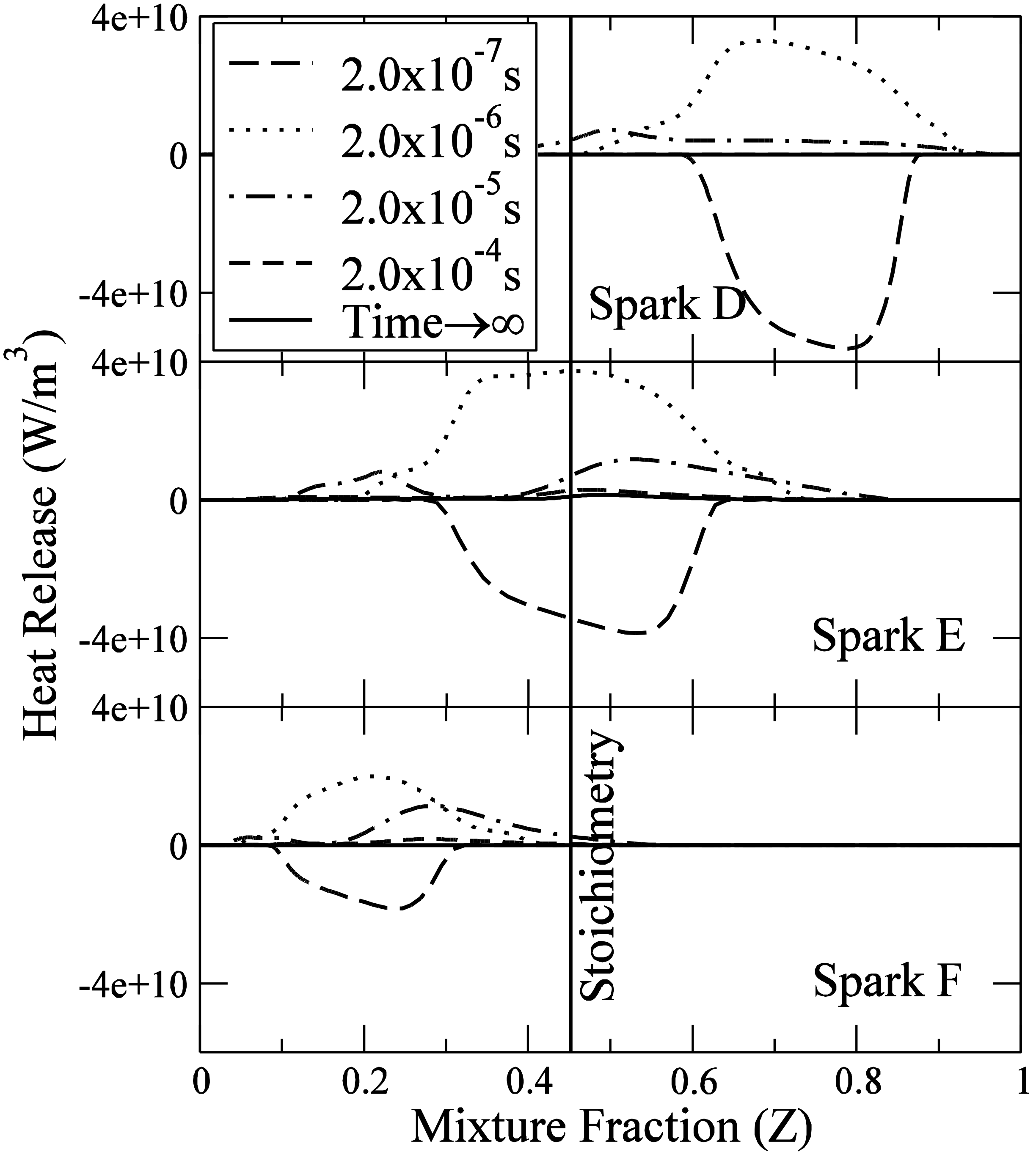
4e+10
0
-4e+10
Heat Release (W/m^3)
2.0x10^{-7}s
2.0x10^{-6}s
2.0x10^{-5}s
2.0x10^{-4}s
Time→∞
Spark D
Spark E
Spark F
Stoichiometry
0
0.2
0.4
0.6
0.8
1
Mixture Fraction (Z)

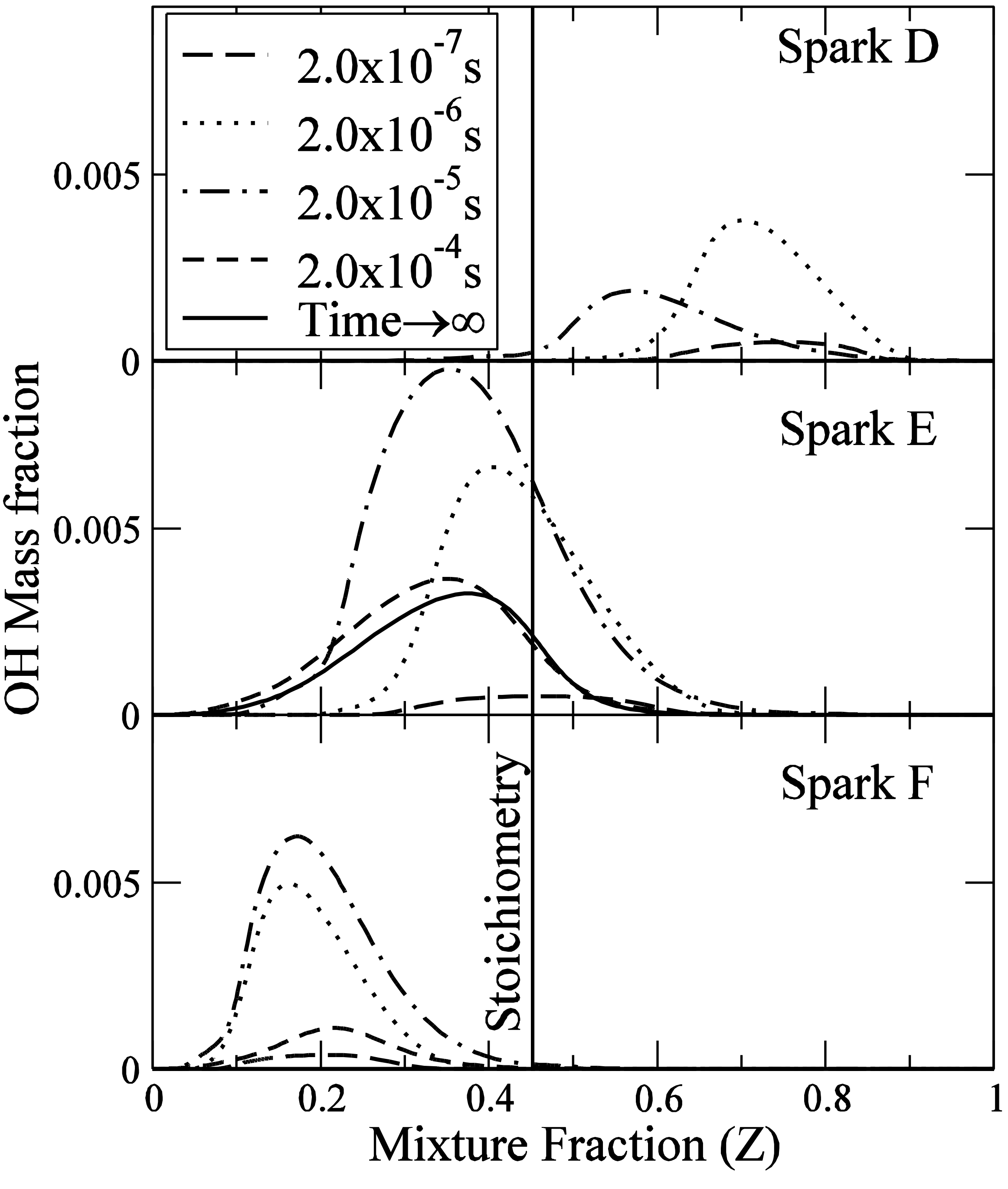
2.0x10^{-7}s
2.0x10^{-6}s
2.0x10^{-5}s
2.0x10^{-4}s
Time→∞
Spark D
Spark E
Spark F
Stoichiometry
OH Mass fraction
0.005
0
0.005
0
0.005
0
0
0.2
0.4
0.6
0.8
1
Mixture Fraction (Z)